Prepublication of
Feero, M. A., Goodfellow, S. D., Lavoie, P., & Sullivan, P. E. (2014). Flow Reattachment Using Synthetic Jet Actuation on a Low-Reynolds-Number Airfoil. AIAA Journal, 1–10.
doi:10.2514/1.J053605

Flow Reattachment Using Synthetic Jet Actuation on a Low Reynolds Number Airfoil

Mark A. Feero*, Sebastian D. Goodfellow†, Philippe Lavoie‡ and Pierre E. Sullivan§

University of Toronto, Toronto, Ontario, Canada

Wind tunnel experiments are used to study the effect of momentum coefficient and excitation frequency on flow separation using synthetic jet actuation. Experiments are conducted on a NACA 0025 airfoil at a chord-based Reynolds number of 100,000 and angle-of-attack of 10°. The actuator is located near the leading edge, downstream of the mean separation location. High-frequency excitation is able to reattach the flow and eliminate the large-scale vortex shedding in the wake, leading to a decrease in drag of approximately 45%. Low-frequency excitation is employed to target the instabilities associated with the separated shear layer and vortex shedding in the wake. Excitation of the wake instability also causes the flow to reattach, however it leads to organization of the large-scale vortex shedding. By forcing the boundary layer at the frequency of the shear layer instability, the threshold momentum required to reattach the flow is an order of magnitude smaller as compared with high-frequency excitation and the large-scale vortex shedding is suppressed.

*PhD Student, Institute for Aerospace Studies, m.feero@mail.utoronto.ca

†PhD Student, Civil Engineering, sebi.goodfellow@mail.utoronto.ca

‡Professor, Institute for Aerospace Studies, lavoie@utias.utoronto.ca

§Professor, Mechanical and Industrial Engineering, sullivan@mie.utoronto.ca

Nomenclature

c	Chord length
C_D	Drag coefficient
C_p	Pressure coefficient
C_μ	Momentum coefficient ($\equiv \overline{U_j}^2 d/0.5U_\infty^2 c$)
d	Synthetic jet slot width
DC	Duty cycle
$E_{u_j u_j}$	Power spectral density of synthetic jet velocity
E_{vv}	Power spectral density of v
f	Frequency
F^+	Reduced excitation frequency ($\equiv f_e X_{sep}/U_\infty$)
L	Streamwise distance from the synthetic jet to the measurement location
Re_c	Chord-based Reynolds number
St	Dimensionless frequency expressed as a Strouhal number ($\equiv fc/U_\infty$)
t	Time
t'	Normalized time ($\equiv (t-\tau)U_\infty/L$)
t^+	Dimensionless reattachment time
u, v	Instantaneous velocity in the steamwise and cross-stream directions, respectively
U	Mean streamwise velocity
$U_\circ$	Mean streamwise outside the airfoil wake at a given downstream location
$\overline{U_j}$	Mean jet velocity over the expulsion half-cycle
U_{min}	Minimum value of U in the airfoil wake
U_∞	Freestream velocity
V_{app}	Synthetic jet voltage amplitude
W_{vv}	Wavelet power spectrum of v
x, y	Streamwise and cross-stream coordinates, respectively

x^*	Local airfoil coordinate aligned with the chord line
X_{sep}	Separated flow domain length
α	Angle of attack
τ	Control initiation time

Subscripts

c	Carrier frequency
e	Excitation frequency
m	Modulation frequency
ws	Dominant wake frequency, separated flow
wa	Dominant wake frequency, attached flow
sl	Dominant shear layer frequency

1 Introduction

The operation of airfoils at low Reynolds number is of interest in a number of engineering applications including low-speed unmanned aerial vehicles, wind turbines, and low-speed/high-altitude aircraft. Standard airfoil profiles are designed for optimal aerodynamic performance at high Reynolds number where inertial forces dominate the flow. At chord based Reynolds numbers less than 10^6, airfoil performance is significantly reduced [1]. Flow separation on airfoils is particularly prevalent at low Reynolds number due to the interaction of the laminar boundary layer on the suction surface with an adverse pressure gradient. The momentum contained in the boundary layer is often unable to withstand the forces imposed by the adverse pressure gradient, which causes the flow to separate near the leading edge.

The use of periodic excitation applied locally at the surface to mitigate flow separation and restore the aerodynamic performance of stalled airfoils is a technique that has been applied with varying degrees of success for a number of years [2]. A common zero-net-mass-flux fluidic actuator for flow control is the synthetic jet. A synthetic jet actuator (SJA) is composed of a vibrating diaphragm mounted in a cavity

with an orifice/slot leading to the surface where control is desired. Deformation of the diaphragm causes the working fluid to be alternately ingested and expelled by the cavity, thereby adding momentum (but not mass) to the flow [3]. The net momentum transferred to the flow during the expulsion phase is due to the formation of a vortex pair at the orifice/slot edge(s).

An extensive review by Greenblatt and Wygnanski [4] concluded that the majority of investigations using periodic excitation on airfoils described an optimum dimensionless frequency within the range $0.3 < F^+ < 4$, where $F^+ = f_e X_{sep}/U_\infty$, f_e is the excitation frequency and X_{sep} is the length of the separated flow domain. This range of F^+ corresponds to an excitation Strouhal number $St_e = f_e c/U_\infty$ that is $\mathcal{O}(1)$. Post-stall separated flow has two dominant features: shear layer roll-up near the leading edge and large scale vortex shedding in the wake [5]. These instabilities are coupled due to the fact that vortex shedding in the wake causes global changes in circulation. Tian et al. [6] demonstrated that the frequency of the shear layer instability (f_{sl}) is larger than that of the separated wake instability (f_{ws}), and the coupling between the two instabilities is non-linear. Excitation of the separated shear layer at $St_e \approx \mathcal{O}(1)$ has proven to be effective since the frequency associated with the separated wake instability, $St_{ws} = f_{ws} c/U_\infty$, is also $\mathcal{O}(1)$. However, Amitay and Glezer [7] demonstrated flow reattachment and performance improvement on a stalled airfoil for both $St_e \approx \mathcal{O}(1)$ and for excitation frequencies an order of magnitude larger, $St_e \approx \mathcal{O}(10)$. For St_e that is $\mathcal{O}(1)$, large vortical structures are formed and convect downstream near the airfoil surface, leading to unsteady reattachment and time-periodic variations in circulation [8]. Actuation at $St_e \approx \mathcal{O}(10)$ is essentially time invariant relative to the time scale of the flow and leads to local modification of the apparent aerodynamic shape of the flow surface, thereby changing the pressure gradient and suppressing flow separation [9]. Similar results were demonstrated by Glezer et al. [10] on a circular cylinder experiencing boundary layer separation at a Reynolds number of 7.55×10^4 based on cylinder diameter. The authors showed that low-frequency excitation caused cross-stream oscillations of the separated shear layer and strong coupling to the wake, while high-frequency excitation displaced the cross-flow and lead to a favourable pressure gradient and more stable boundary layer.

Due to their compact size, piezoelectric disks are commonly used as the oscillating diaphragm(s) for synthetic jet actuators mounted inside aerodynamic bodies. The relatively small cavities that house the

piezoelectric diaphragms often lead to optimum synthetic jet excitation frequencies that are well above the dominant frequencies of the flow. Therefore, modulation of high-frequency control signals has been employed and demonstrated as an effective method to target low frequencies that are outside the bandwidth of SJAs. Amitay and Glezer [7] and Pinier et al. [11] used amplitude modulation to control flow separation and target frequencies that are $St = fc/U_\infty \approx \mathcal{O}(1)$, while Glezer et al. [10] employed burst modulation. Tian et al. [6] compared the ability of amplitude and burst modulated control signals to increase the lift-to-drag ratio on a stalled NACA 0025 airfoil and found that the two strategies produced similar benefits, while burst modulation required significantly less energy to do so.

The effect of excitation amplitude for SJAs is characterized using the momentum coefficient, C_μ, defined as the ratio of the time-averaged momentum of the synthetic jet to the momentum of the freestream, *viz.*

$$C_\mu = \frac{\overline{U_j}^2 d}{0.5 U_\infty^2 c}, \tag{1}$$

where d is the orifice diameter/slot width, and $\overline{U_j}$ is the mean jet velocity over the expulsion half of the cycle. Amitay et al. [9] investigated the influence of C_μ on separation control of a circular-leading-edge NACA airfoil operation between $3.1 \times 10^5 < Re_c < 7.25 \times 10^5$ using a pair of SJAs. The authors found that C_μ on the order $\mathcal{O}(10^{-3})$ was required to cause the flow to reattach. Tian et al. [6] used both amplitude-modulated and burst-modulated synthetic jet actuation to optimize the lift-to-drag ratio on a post-stalled NACA 0025 airfoil at $Re_c = 10^5$ and angle-of-attack $\alpha = 20°$. A closed-loop control strategy was able to fully reattach the flow and increase lift-to-drag by a factor of 2 for $C_\mu \approx \mathcal{O}(10^{-5}) - \mathcal{O}(10^{-4})$. Goodfellow et al. [12] found that a SJA was able to decrease drag by 64% on a NACA 0025 airfoil operating at $Re_c = 10^5$ and $\alpha = 5°$ when C_μ reached a threshold value that was $\mathcal{O}(10^{-3})$. Below the threshold value, negligible gain in aerodynamic performance was achieved.

It has previously been observed that for a given excitation frequency, once a threshold value of C_μ has been established, further increasing the excitation amplitude provides relatively small benefits in terms of increasing lift or decreasing drag on a stalled airfoil [4, 9]. This is likely attributed to the fact that the flow has already been reattached. However, it is unclear what effect St_e may have on the threshold value of C_μ for flow reattachment. Nishri and Wygnanski [13] showed that for a deflected flap, the smallest threshold

C_μ was achieved for $F^+ \approx 1$ for a range of Reynolds numbers. The situation increases in complexity for an airfoil experiencing laminar boundary layer separation where several dominant instabilities are present. The goal of the current work was to investigate the influence of excitation amplitude (C_μ) and frequency (St_e) on flow reattachment and drag reduction on a stalled airfoil using synthetic jet actuation. High-frequency ($St_e \approx \mathcal{O}(10)$) excitation was compared to low-frequency ($St_e \approx \mathcal{O}(1)$) excitation, which targeted the shear layer and global wake instabilities. The momentum coefficient was varied from $\mathcal{O}(10^{-4}) - \mathcal{O}(10^{-2})$ for each excitation strategy. Measurements of the synthetic jet velocity were performed and are included to provide the required information about the forcing imparted by the actuator.

2 Experimental setup

Experiments were conducted in a low-speed recirculating wind tunnel with a 5 m long octagonal test section that is 0.91 m wide and 1.22 m tall. Low-turbulence flow entered the test section after passing seven screens and a 9:1 contraction. The freestream velocity in the test section is monitored using a static pitot tube located at the test section inlet. The tunnel was operated at a freestream velocity of approximately $U_\infty = 5$ m/s for $Re_c = 10^5$. The freestream turbulence intensity at the airfoil for $U_\infty = 5$ m/s is 0.22%.

Experiments were performed on a NACA 0025 airfoil with a chord length of $c = 300$ mm that spanned the width of the test section. This airfoil geometry is representative of those used in low Reynolds number wind turbine blades, which typically require relatively thick airfoil profiles to withstand the large aerodynamic loads. The airfoil was mounted $1.33c$ downstream of the inlet to the test section and pivoted about the quarter-chord location to adjust the angle-of-attack relative to the freestream velocity, α, which was fixed at $\alpha = 10°$. The Reynolds number of 100,000 and angle-of-attack 10° were selected based on previous work that showed that under these conditions, the boundary layer separates from the suction surface and fails to reattach [14]. The solid blockage ratio of the model at $\alpha = 10°$ was 7.4%. The model had 65 static pressure taps distributed evenly between the upper and lower surfaces at mid-span. Aerodynamic $\alpha = 0°$ was identified as the rotation angle of the airfoil that corresponded to a symmetric pressure coefficient (C_p) distribution. These pressure measurements were performed using a Scanivalve 64-port pressure scanner connected to an MKS 226A Baratron pressure transducer. The C_p distribution at $\alpha = 0°$ is shown in Figure 1a, where x^* is

the chordwise coordinate with $x^* = 0$ located at the leading edge of the airfoil (note that data at $x^*/c = 0.76$ on the suction surface is excluded due to a damaged pressure tap).

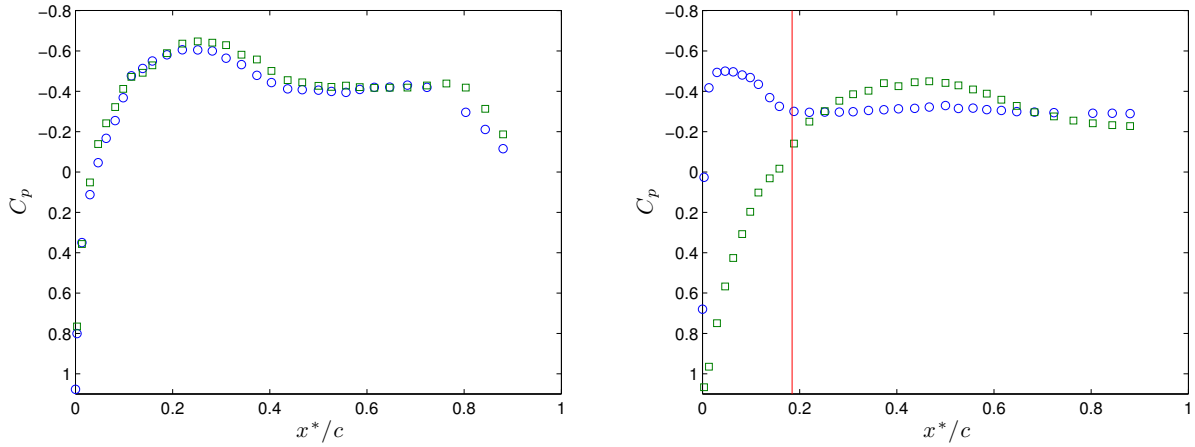

(a) (b)

Figure 1: Pressure coefficient distributions at $Re_c = 10^5$ for (a) $\alpha = 0°$ and (b) $\alpha = 10°$. (○) and (□) symbols correspond to the suction and pressure surfaces, respectively. Separation occurs for $\alpha = 10°$ at $x^*/c = 0.18$ and is noted with the vertical line in Figure 1b.

The SJA was driven by four axisymmetric Thunder TH-5C piezoelectric actuators from Face International Corporation. Oscillation of the piezoelectric actuators inside the cavity causes air to be alternately expelled and ingested through a high aspect ratio slot that is 140 mm long and 0.5 mm wide. The four piezoelectric actuators were operated in phase and it was verified experimentally that the velocity across the slot length was in phase to within ±5°. As seen in Figure 2, the actuators are mounted on the side wall of the cavity such that their motion is perpendicular to the motion of the fluid in the slot. This type of synthetic design is common for actuators mounted inside aerodynamic bodies (e.g., [15, 16]). The input signal to the SJA was from a Rigol DG1022 function generator and was amplified by a Mide QPA3202 voltage amplifier. A slot in the airfoil surface offset to one side of the pressure taps allowed the chordwise location of the SJA to be varied from $x^*/c = 0.19$ to 0.34. With the SJA in place, the remainder of the slot was covered by a removable cap that was machined to match the airfoil curvature. At $\alpha = 10°$, the flow separated at approximately $x^*/c = 0.18$ (Figure 1b). The average separation point was estimated as the x^*/c location

corresponding to the beginning of a region of constant static pressure [17]. The jet was located approximately $0.01c$ downstream of the mean separation point at its most upstream position (the position used in these experiments). Figure 3 shows a schematic of the synthetic jet actuator positioned inside the airfoil and defines the global coordinate system.

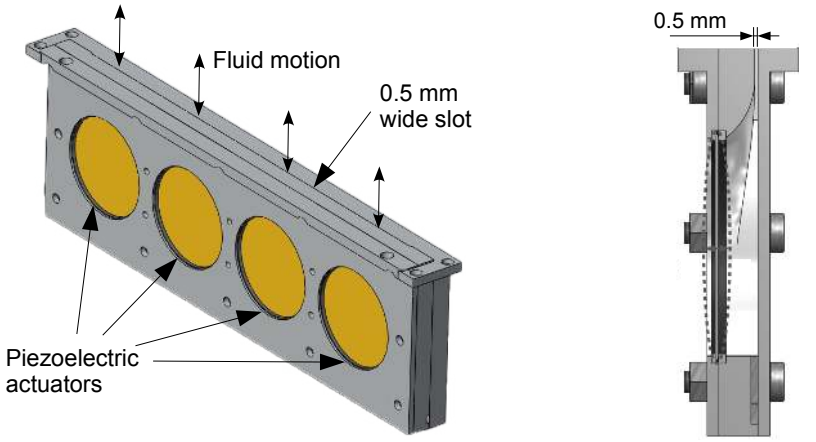

(a) Solid model. (b) Cross-section.

Figure 2: Synthetic jet actuator details.

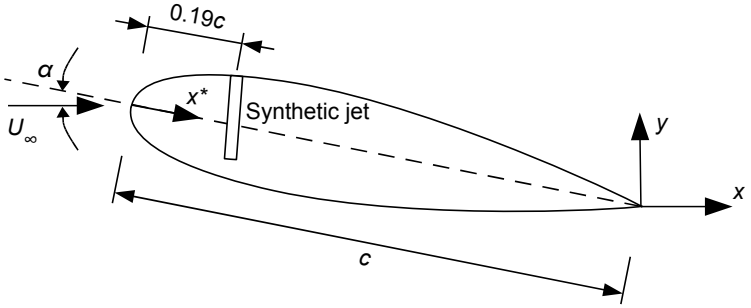

Figure 3: NACA 0025 airfoil model with synthetic jet actuator.

Flow velocity was measured using constant temperature hot-wire anemometry. A Dantec 56C01 main unit with 56C17 CTA bridges was used with single and cross-wire probes. The hot-wire probes were 5 μm tungsten wire plated with copper with a sensing length of 1 mm. For the cross-wire probes, the wire angles were approximately $\pm 45°$ and the spacing between prongs was 4 mm. Single-wire calibration data was fit according to King's Law and data reduction for cross-wire probes was accomplished using a lookup-table

technique. The measurement uncertainty for all mean and fluctuating velocity quantities presented was approximately 3% based on the error propagation methodology of Yavuzkurt [18]. Spectral analysis of the cross-stream velocity was used to identify dominant frequency characteristics of the near wake. For each power spectrum, 2^{21} data points were acquired and windowed into 256 overlapping segments each containing 2^{13} points. A sampling frequency of 5 kHz was used for all spectral measurements, giving a frequency resolution of 0.61 Hz. The power spectral density (PSD) of individual segments were computed and averaged.

The impact of synthetic jet actuation on the aerodynamic performance of the airfoil was evaluated by the reduction in the drag coefficient relative to the baseline case. The section drag force was determined using a control volume approach from [19, 20],

$$C_D = -\frac{2}{U_\infty^2 c}\int_{y_1}^{y_2}[U(U-U_\infty) + (\overline{u'}^2 - \overline{v'}^2)]\,dy, \tag{2}$$

where $\overline{u'}$ and $\overline{v'}$ are the rms values of the streamwise and cross-stream fluctuating velocity components, respectively, and y_1 and y_2 are the lower and upper bounds of the measurement plane. This formulation of the drag coefficient differs slightly from Antonia and Rajagopalan [19] as it strictly applies mass conservation across the control volume boundaries. This method of determining drag is recommended for wing-like bodies where the drag force is dominated by the momentum-flux at the control volume boundaries [21]. Often, $\overline{u'} \approx \overline{v'}$ and the fluctuating velocity term in (2) can be ignored. Wake surveys used in the calculation of C_D were performed at $x/c = 2$. The streamwise location of this measurement plane is consistent with other studies concerning thick, stalled airfoils [7, 22, 23]. Wake profiles from $y/c = -0.81$ to 1.03 were measured in steps of $0.042c$ using either single or cross-wire probes mounted on a three-axis traverse.

3 Results

3.1 Synthetic jet characterization

Prior to the flow control experiments with the SJA installed in the airfoil, the response of the exit-plane jet velocity to sinusoidal excitation was characterized in quiescent conditions. The SJA was clamped in a rigid stand and a single hot-wire probe was positioned at the centre of the slot exit-plane. The jet velocity was

measured at a spanwise location corresponding to the centreline of one of the piezoelectric actuators. The hot-wire dimensions were as described in Section 2 and data was sampled at 20 kHz. The SJA was driven at frequencies ranging from $f_e = 200$ Hz to 1200 Hz and voltage amplitudes from $V_{app} = 50$ to 350 V (peak-to-peak) in 50 V intervals. Preliminary measurements showed that the jet velocity was outside the calibration range below $f_e = 200$ Hz (< 0.5 m/s) and therefore characterization for the full range of voltage amplitudes was performed at frequencies ≥ 200 Hz. Phase averaged velocity cycles for each case were computed from 4848 individual cycles with a phase resolution of 1.8°. The phase averaged velocity was converged to within 1% at the 95% confidence interval over the entire cycle in all cases.

The response of $\overline{U_j}$ to sinusoidal excitation is shown in Figure 4. Note that the synthetic jet was characterized in quiescent conditions and it was assumed that the exit-plane jet velocity would be unchanged when operating in cross-flow. While there is likely to be some change in the jet velocity, particularly during the ingestion portion of the cycle, characterization of the jet in cross flow is difficult and a bench-top calibration is common practice (e.g. [9, 24, 11]). Figure 4 shows that at each excitation amplitude, a resonant peak is seen at $f_e \approx 970$ Hz. The characterization of the jet was restricted to frequencies below $f_e = 1200$ Hz due to limitations of the voltage amplifier at $V_{app} \geq 300$ V and $f_e \geq 1200$ Hz. A measurement at $V_{app} = 100$ V for $f_e = 50 - 2700$ Hz performed by Goodfellow [25] confirmed that a second resonant peak exists at approximately 2500 Hz, however this resonant peak has significantly lower amplitude. Excitation at $f_e = 970$ Hz provides a broad range of control authority for the wind tunnel experiments performed at $U_\infty = 5$ m/s since the jet velocity can be varied from values that are much smaller than U_∞ (low-amplitude excitation) to values near $4U_\infty$. In terms of momentum coefficient, C_μ spans almost three orders of magnitude at $f_e = 970$ Hz for $U_\infty = 5$ m/s and $c = 300$ mm. Furthermore, $f_e = 970$ Hz corresponds to an excitation Strouhal number $St_e = 72$ and is therefore appropriate for high-frequency excitation. This frequency was selected as the optimal excitation frequency of the SJA. Since the jet velocity decreases rapidly as the excitation frequency is reduced below 970 Hz, a low-frequency excitation strategy will be discussed in Section 3.3.

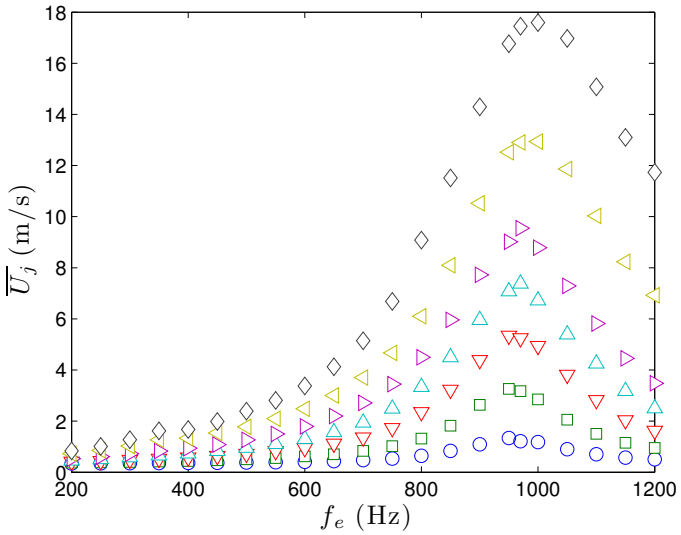

Figure 4: Mean jet velocity, $\overline{U_j}$, versus excitation frequency for increasing voltage amplitude. ($\circ$) V_{app}=50 V, ($\square$) V_{app}=100 V, ($\triangledown$) V_{app}=150 V, ($\triangle$) V_{app}=200 V, ($\triangleright$) V_{app}=250 V, ($\triangleleft$) V_{app}=300 V, ($\diamond$) V_{app}=350 V.

3.2 Aerodynamic control: High St

Mean streamwise velocity profiles in the wake of the airfoil at $\alpha = 10^\circ$ and $Re_c = 10^5$ for increasing C_μ are shown in Figure 5 normalized by U_o, the mean outer flow velocity. Sufficient data were acquired for all velocity measurements such that U was converged to within 0.1%. C_μ was varied from 0.018% to 3.72% by increasing the applied voltage for harmonic excitation at $St_e = 58$. In the uncontrolled case, the wake extended from approximately $y/c = -0.25$ to 0.7, giving an uncontrolled wake width of $0.95c$. As expected, the cross-stream location of the minimum velocity is above the trailing edge of the airfoil since the boundary layer on the suction surface separates near the leading edge and fails to reattach. The minimum velocity $U_{min} = 0.85U_o$ occurs $0.28c$ above the trailing edge. As C_μ is increased to 0.018% and 0.12%, the flow remains separated and the mean velocity profile is relatively unchanged. However, when $C_\mu = 0.34\%$, the wake is deflected down such that U_{min} occurs at $y/c \approx 0$ and the wake width decreases to $0.57c$. The minimum velocity also increases slightly to $U_{min} = 0.88U_o$. These changes indicate partially or completely reattached flow. As C_μ was increased, little change was observed in the wake as the flow had already reattached. To confirm these findings, flow visualization of the flow over the airfoil and in the near wake was performed

using a smoke-wire located $\sim 0.5c$ upstream of the leading edge. As shown in Figure 6, flow visualization showed the airfoil boundary layer remained separated for $C_\mu = 0.018\%$ and 0.12%, and became reattached when $C_\mu \geq 0.34\%$. A noticeably narrower wake is observed in Figure 6(d)-(h).

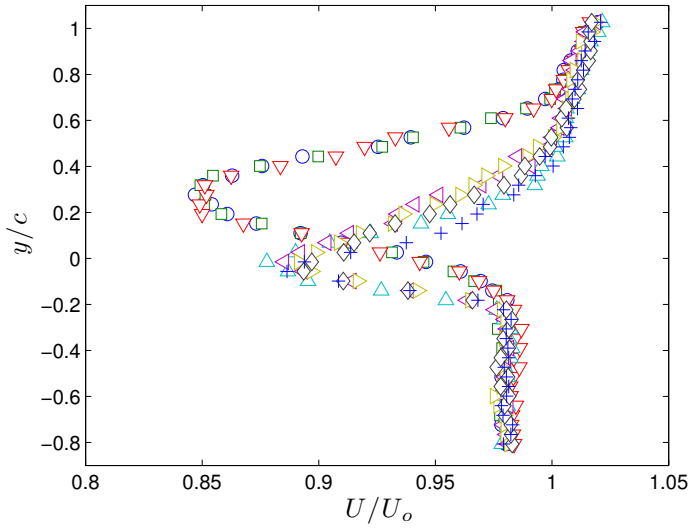

Figure 5: Mean streamwise velocity at $x/c = 2$. ($\circ$) $C_\mu = 0$, ($\square$) $C_\mu = 0.018\%$, ($\triangledown$) $C_\mu = 0.12\%$, ($\triangle$) $C_\mu = 0.34\%$, ($\triangleleft$) $C_\mu = 0.66\%$, ($\triangleright$) $C_\mu = 1.11\%$, ($\Diamond$) $C_\mu = 2.03\%$, ($+$) $C_\mu = 3.72\%$.

(a) $C_\mu = 0$

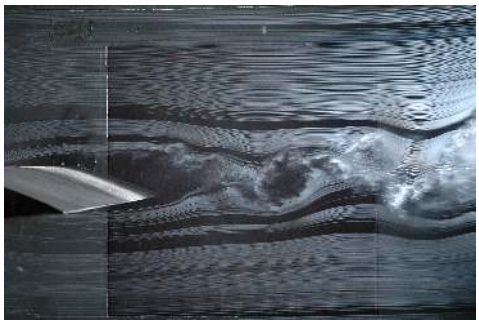

(b) $C_\mu = 0.018\%$

(c) $C_\mu = 0.12\%$

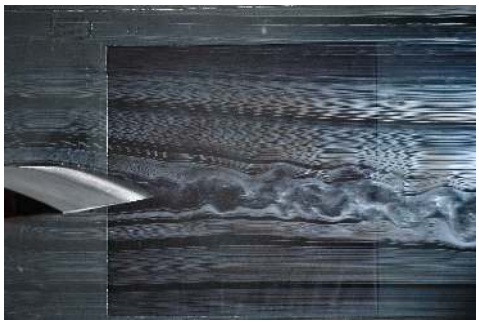

(d) $C_\mu = 0.34\%$

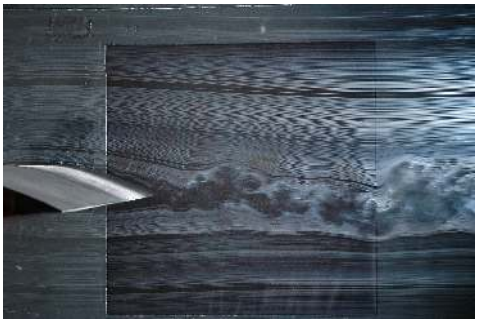

(e) $C_\mu = 0.66\%$

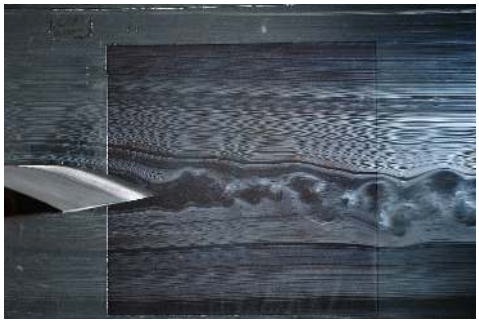

(f) $C_\mu = 1.11\%$

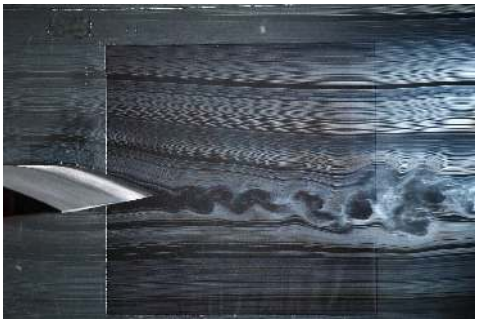

(g) $C_\mu = 2.03\%$

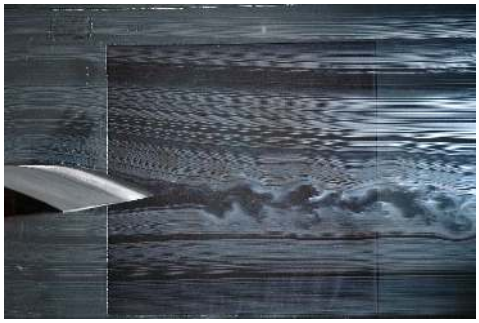

(h) $C_\mu = 3.72\%$

Figure 6: Flow visualization in the near wake.

The fluctuating velocity term in (2) can be ignored when $\overline{u'} \approx \overline{v'}$ over the entire measurement plane. Figure 7 shows $\overline{u'}$ and $\overline{v'}$ measured at $x/c = 2$ for (a) the baseline case with separated flow, and (b) $C_\mu = 0.34\%$ where the flow is attached. At the 95% confidence interval, $\overline{u'}$ and $\overline{v'}$ were converged to within 0.5% according to the bootstrap resampling algorithm from Benedict and Gould [26]. Since $\overline{u'}$ and $\overline{v'}$ are approximately equal over the span of the measurement plane in each case, the fluctuating term in (2) can be neglected and C_D is calculated using only the momentum term, *viz.*

$$C_D = -\frac{2}{U_\infty^2 c} \int_{y_1}^{y_2} U(U - U_\infty)\, dy, \tag{3}$$

which is equivalent to the wake profile method developed by Jones [27]. The difference between C_D calculated using (2) and (3) for $C_\mu = 0$ (Figure 7a) is 3%.

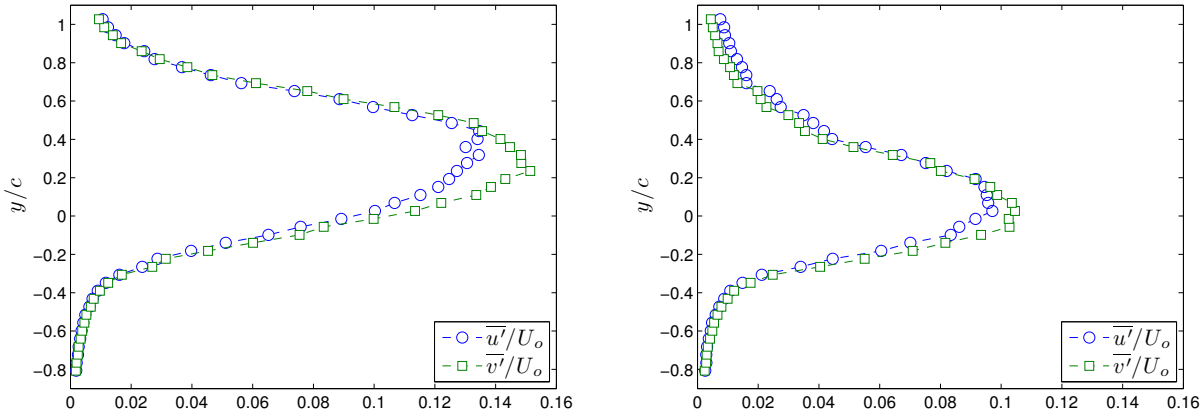

(a) $C_\mu = 0$.

(b) $C_\mu = 0.34\%$.

Figure 7: Mean fluctuating velocity components measured at $x/c = 2$ for (a) separated and (b) reattached flow.

The impact of excitation at $St_e = 58$ on the airfoil drag coefficient, C_D, for increasing C_μ is shown in Figure 8. C_D was normalized by the drag coefficient of the unexcited case ($C_\mu = 0$) to highlight the relative change in drag. For $C_\mu < 0.34\%$ there is little change in C_D, since the flow remains separated. As C_μ increased to 0.34%, the flow reattaches and a significant decrease in C_D of $\sim 45\%$ is observed. Increasing C_μ to 3.72% caused an additional change of $\sim 10\%$, although it initially increased for intermediate values of

C_μ. This modest change in C_D for higher C_μ is because the flow had already attached and suggests that the effectiveness of excitation at high St_e on drag reduction depends primarily on exceeding a threshold value of C_μ. Figure 8 compares the results of Goodfellow et al. [12] at $\alpha = 5°$ on the same airfoil for $Re_c = 10^5$. These results show a similar trend and demonstrate the threshold C_μ is approximately equal for $\alpha = 5°$ and 10°, however a larger decrease in drag is possible for 5°. This is likely due to the fact that a more severe adverse pressure gradient is present on the suction surface of the airfoil at $\alpha = 10°$.

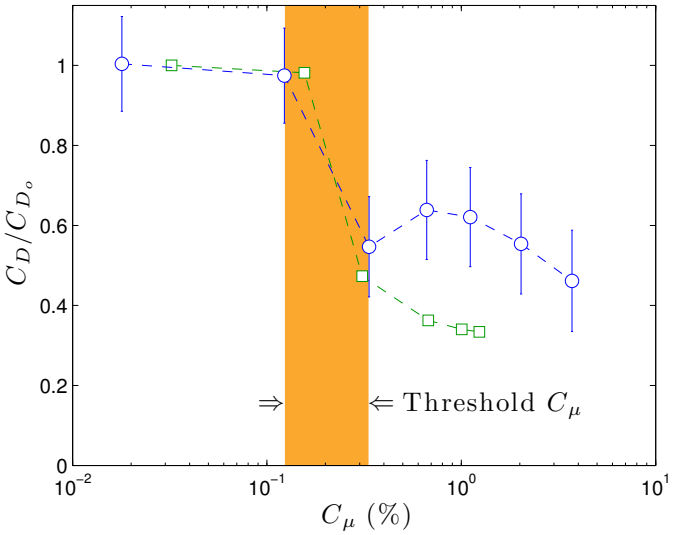

Figure 8: C_D as a function of C_μ for (○) $\alpha = 10°$ and (□) $\alpha = 5°$. Data for $\alpha = 5°$ are from Goodfellow et al. [12]. The shaded area indicates the threshold range of C_μ required to cause flow reattachment. Error bars represent the relative measurement uncertainty.

Spectral analysis of the cross-stream velocity was performed at a y/c location on the lower side of the airfoil corresponding to the half-width of the wake where the velocity deficit is half the maximum deficit. This location remained approximately constant depending on the state of the flow (i.e. separated or attached). The power spectra of v at $x/c = 1$ are shown in Figure 9 (successive spectra are stepped by an order of magnitude for clarity). When the flow is fully separated, a broad peak associated with vortex shedding in the wake is centred at $St_{ws} = 0.84$ ($f_{ws} = 14$ Hz), in agreement with the typical separated wake frequency $St_{ws} \approx \mathcal{O}(1)$ reported in the literature. The large scale vortex shedding associated with St_{ws} can be seen in the smoke wire images in Figures 6(a), (b) and (c). As the flow becomes reattached at $C_\mu = 0.34\%$, the

broad peak at St_{ws} is flattened and the decay in the spectra is delayed. From classical scaling arguments, the dominant frequency associated with the wake should be proportional to U_∞ and inversely proportional to the width of the wake [28]. Therefore, as the flow over the airfoil is reattached and the wake becomes narrower, the dominant frequency of the wake is expected to increase. An example of this behaviour was demonstrated by Yarusevych et al. [14], where the flow over a NACA 0025 airfoil at $\alpha = 5°$ was reattached by increasing Re_c. Figure 9 shows that as C_μ is increased beyond the threshold value, a distinct peak in the spectra associated with the attached flow begins to emerge at $St_{wa} = 4.86$ when C_μ reaches 2.03%. Evidence of these structures with reduced spatial scale can be seen in Figures 6(g) and (h).

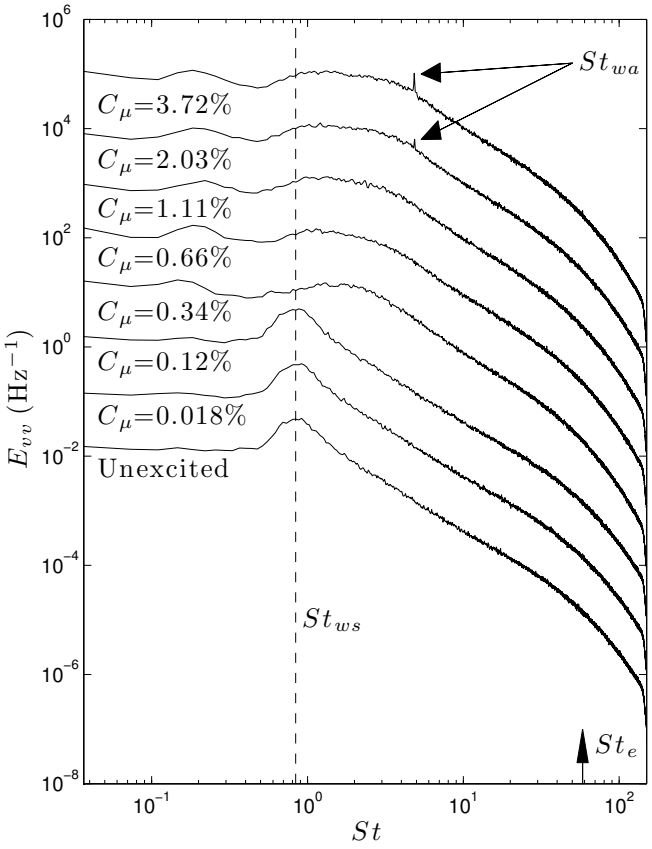

Figure 9: PSD of v at $x/c = 1$ for increasing C_μ and high-frequency excitation at $St_e = 58$. Successive spectra are stepped by an order of magnitude for clarity.

Temporal characteristics of the reattachment process were investigated by measuring the frequency content

of the wake subjected to a control signal that is zero and then switched to $C_\mu = 3.72\%$ at time $t = \tau$. The velocity was measured at $x/c = 1$ and $y/c = -0.07$, a location that corresponds to the edge of the shear layer when the flow is separated and the half-width of the wake when the flow is attached. A continuous wavelet transform with a Morlet mother wavelet was used to compute the time dependent frequency content of the wake. Figure 10 shows the phase-averaged magnitude of the wavelet power spectrum for the cross-stream velocity component, W_{vv}. Phase-averaged wavelet spectra were computed from 200 independent measurements. The wavelet power spectrum is plotted against a normalized time variable $t' = (t - \tau)U_\infty/L$, where L is the streamwise distance from the actuator to the measurement location. Included in the plot is a dashed line showing the cone of influence (COI), below which edge effects due to the finite size of the time series become significant. As expected, a distinct peak at St_{ws} is observed prior to $t' = 0$. After control is switched on, a noticeable change in the wake is observed at $t' = 1.3$ by a momentary attenuation of frequencies from $St = 3$ to 6. This is followed by a sharp increase in energy at St_{ws} for $t' = 1.6$ before the vortex shedding associated with the separated flow is completely suppressed. The flow reaches a steady state after an increase in W_{vv} for frequencies from $St \approx 2$ to 4.2 for $t' \approx 3.2$ to 6. Assuming that the time required for information to reach the hot-wire from the actuator is L/U_∞, then any temporal variations in W_{vv} beyond $t' = 1$ are because of the reattachment process. This gives a reattachment time scale of $5L/U_\infty$. In applications involving flow separation, a dimensionless reattachment time, t^+, is conventionally defined using U_∞ and X_{sep}. The time scale of reattachment is $t^+ = 10.9$. This compares well with Siauw et al. [29] and Amitay and Glezer [8] who found $t^+ = 9.5$ and $t^+ = 10$, respectively. The transient behaviour of the peak at St_{ws} has been observed in other investigations and is caused by the starting vortex that occurs during the reattachment process as a result of the step change in circulation when control is initiated [7, 29]. The results shown in Figure 10 further confirm that steady reattachment occurs when high frequency excitation is employed.

3.3 Aerodynamic control: Low St

Low frequency excitation was used to target the two characteristic frequencies associated with the separated flow: f_{ws} and f_{sl}. Yarusevych et al. [30] found that $f_{sl} \approx 165$ Hz for the NACA 0025 airfoil used in this study

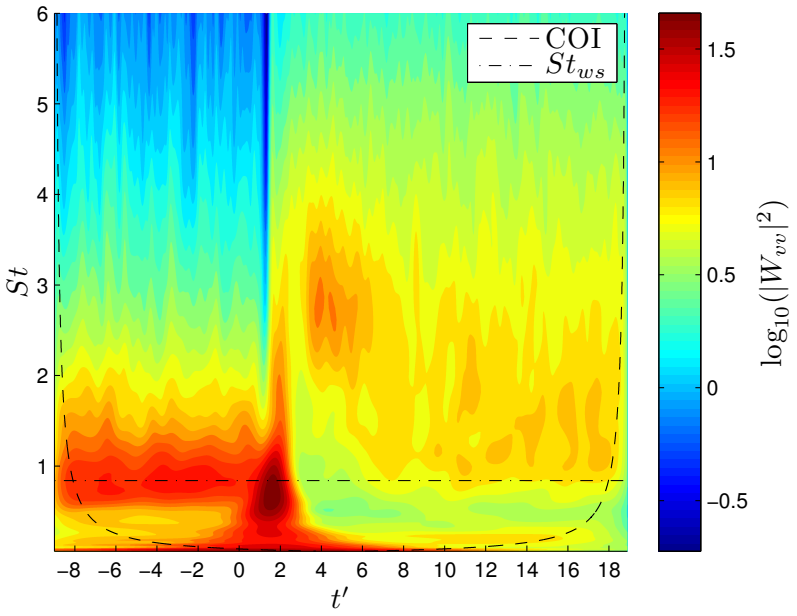

Figure 10: Wavelet power spectrum of v at $x/c = 1$ for excitation $St_e = 58$ and $C_\mu = 3.72\%$.

when operating at $\alpha = 10^\circ$ and $Re_c = 10^5$. The Strouhal number associated with the shear layer frequency is $St_{sl} = 9.9$. Figure **??** shows that below $St_e = 12$, C_μ is relatively small and varies little with input voltage, placing these frequencies outside the effective bandwidth of the SJA. To target low frequencies that are $St \approx \mathcal{O}(1)$, burst modulation of the high-frequency excitation at $St_e = 58$ was used. A burst modulated waveform is composed of a sine wave at a carrier frequency f_c (St_c) modulated by a square wave at f_m (St_m) with duty cycle DC, where $f_m < f_c$. The square wave varies between 0 and 1 such that the sine wave occurs in "bursts". Tian et al. [6] used hot-wire measurements near the synthetic jet slot exit to show that the energy contained in the flow at the modulation frequency was comparable to the energy at the carrier frequency when using amplitude modulation. However, they did not provide similar measurements for burst modulated excitation. Figure 11 shows a typical power spectrum of the SJA exit-plane jet velocity for burst modulated excitation with $f_c/f_m = 60$ and DC=50%. Distinct peaks in the spectra are seen at both f_m and $2f_c$, along with the harmonics of f_m ($2f_m$, $3f_m$, etc.). The harmonics of f_m are due to the digitization of a square-wave signal and are not associated with physical characteristics of the flow produced by the jet. Note that due to rectification of the hot-wire signal in the time-periodic reversing flow of the jet, the frequency

of the carrier signal appears to be $2f_c$ rather than f_c (this was also observed for harmonic excitation of the SJA). The non-linear interaction of the square and sinusoidal waves is apparent by the peaks observed at $2f_c \pm f_m$, $2f_c \pm 2f_m$, etc. These results clearly demonstrate that despite $f_c >> f_m$, there is significant energy contained at the modulation frequency. As long as the carrier frequency is much larger than the largest frequency associated with the flow (f_{sl} in this case), burst modulation is a viable low-frequency excitation technique for targeting frequencies far below the optimum bandwidth of the SJA.

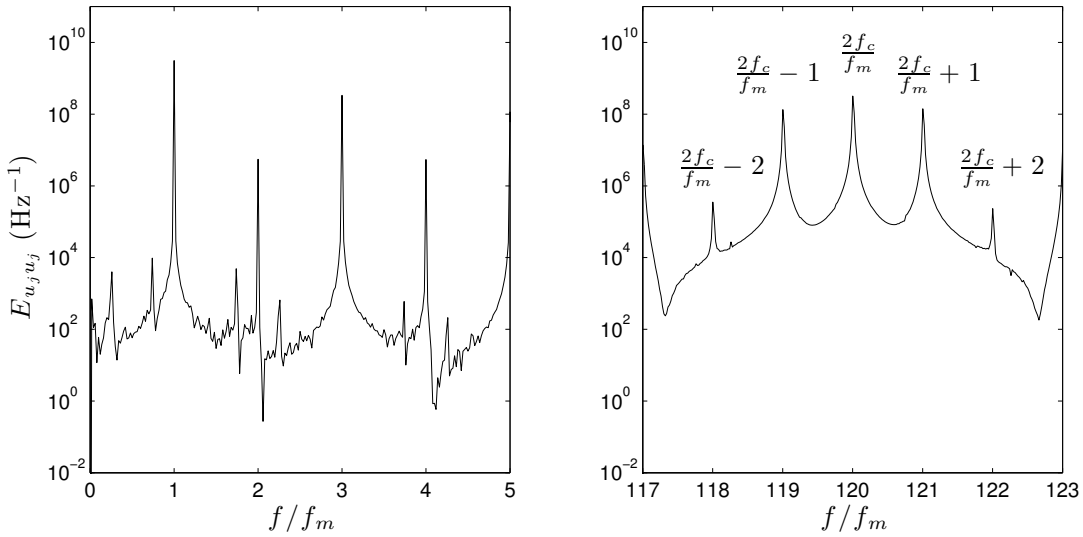

Figure 11: PSD of the synthetic jet velocity measured at the centreline of the jet exit plane for burst modulated excitation with $f_c = 600$ Hz, f_m=10 Hz, DC=50% and $V_{app} = 200$ V.

The effect of low frequency excitation on the mean streamwise velocity in the wake is shown in Figure 12. The carrier frequency and duty cycle were fixed at $St_c = 58$ and DC=50%. Similar to high frequency excitation, excitation at $St_m = St_{ws} = 0.84$ and $St_m = St_{sl} = 9.9$ leads to reattached flow with a narrower wake that is shifted down towards $y/c = 0$ and has a larger value of U_{min} when C_μ exceeds a threshold value. For $St_m = 0.84$, the flow reattached at $C_\mu = 0.12\%$, which is 63% less than the threshold C_μ for harmonic excitation at $St_e = 58$. Increasing C_μ beyond 0.12% had relatively little effect on the shape of the velocity profile. As St_m was increased to 9.9, the flow reattached when $C_\mu = 0.018\%$, the lowest momentum coefficient considered and an order of magnitude smaller than what was required for high frequency harmonic excitation. Compared to larger values of C_μ, the wake profiles at $C_\mu = 0.018\%$ and 0.12% are slightly wider.

No significant change is observed in the mean velocity profiles for $C_\mu \geq 0.34\%$. For both $St_m = 0.84$ and $St_m = 9.9$, flow reattachment causes the minimum velocity to increase to the same value noted for high frequency excitation, $U_{min} \approx 0.88U_o$.

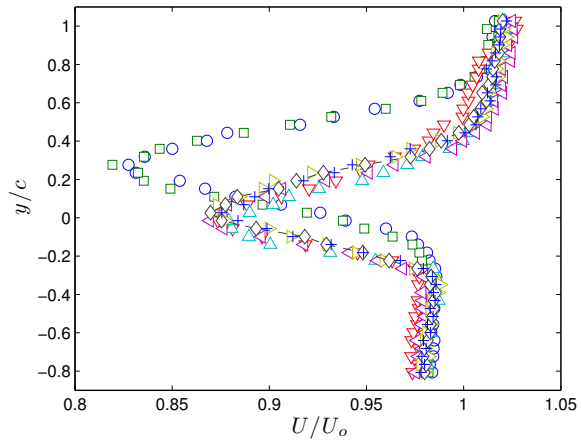

(a)

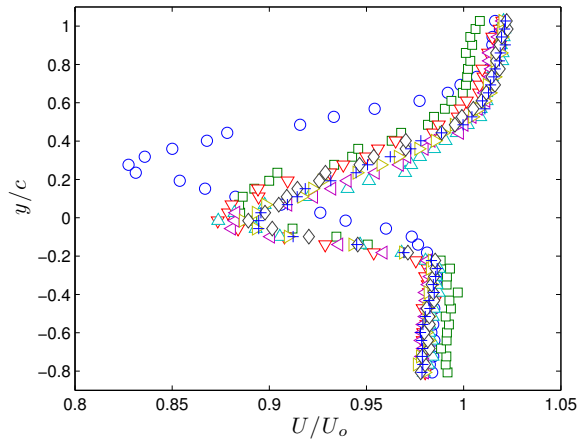

(b)

Figure 12: Mean streamwise velocity at $x/c = 2$ for (a) $St_m = 0.84$ and (b) $St_m = 9.9$. ($\circ$) $C_\mu = 0$, ($\square$) $C_\mu = 0.018\%$, ($\triangledown$) $C_\mu = 0.12\%$, ($\triangle$) $C_\mu = 0.34\%$, ($\triangleleft$) $C_\mu = 0.66\%$, ($\triangleright$) $C_\mu = 1.11\%$, ($\Diamond$) $C_\mu = 2.03\%$, ($+$) $C_\mu = 3.72\%$.

Power spectra of the cross-stream velocity in the wake of the airfoil for burst modulation at $St_m = 0.84$ and $St_m = 9.9$ are shown in Figures 13(a) and (b), respectively. As shown in Figure 13a, the vortex shedding

at St_{ws} persisted for $C_\mu \geq 0.12\%$, which suggests that the flow reattachment is unsteady when $St_m = 0.84$. The narrowing of the initially broad peak at St_{ws} demonstrates that excitation at $St_m = 0.84$ organized the separated wake instability. This evidence of unsteady reattachment and organized vortex shedding in the wake agrees with the time-periodic changes in circulation observed by Amitay and Glezer [8]. As C_μ increases, the peak at St_m increases in magnitude and harmonics up to $4St_m$ emerge. The frequency content of the wake is drastically different for excitation at $St_m = 9.9$ (Figure 13b). No evidence of coherent structures at St_m is observed in the wake, and the same peak associated with attached flow for high frequency excitation, $St_{wa} = 4.86$, begins to emerge and grow in magnitude with increasing C_μ. It is also interesting to note that the peak at St_{wa} begins to appear at $C_\mu = 0.66\%$, compared with $C_\mu = 2.03\%$ for high-frequency excitation (Figure 9). This may be due to more efficient organization of the wake when forcing is applied at $St_m = St_{sl}$. The power spectra suggest that modulation at St_{sl} appears to be more effective in suppressing the large-scale vortex shedding in the wake associated with the separated flow.

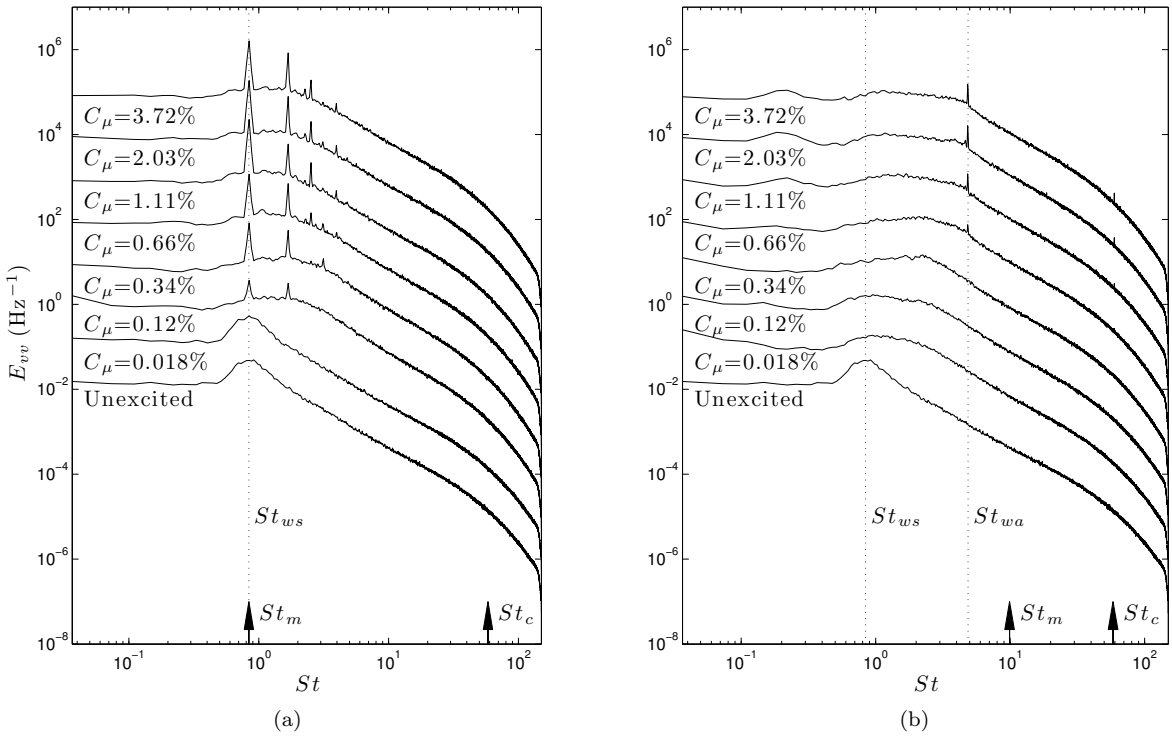

Figure 13: PSD of v at x/c=1 for $St_c = 58$ and (a) St_m=0.84 and (b) St_m=9.9.

Figure 14a compares the variation in C_D with C_μ for the three excitation frequencies considered in this work. For $St_m = 0.84$, there is an initial increase in C_D due to the organization of the vortex shedding at St_{ws}. As C_μ is increased to 0.12%, the threshold momentum coefficient required for reattachment is reached and C_D is decreased by ∼30%. A similar decrease in C_D is observed for St_m=9.9, however it is achieved for the lowest C_μ considered, 0.018%. At $C_\mu = 0.34\%$, all three excitation strategies reach a minimum value of C_D and continuing to increase C_μ has little effect. Harmonic excitation at St_e=58 performs marginally better at the largest value of C_μ, however the energy required is double that of burst modulation with DC=50%. The results in Figure 14a demonstrate that appreciable drag reduction can be achieved for a smaller threshold C_μ when burst modulation is employed at either $St_m = St_{ws}$ or $St_m = St_{sl}$. However, the results also suggest that the value of C_μ required for maximum drag reduction is independent of St_m. A possible explanation for the common minimum in C_D for all excitation strategies may be inferred from the unsteady blowing ratio, $\overline{U_j}/U_\infty$, as shown in Figure 14b. While the threshold C_μ values for drag reduction occur at arbitrary values of $\overline{U_j}/U_\infty$, the minimum drag occurs at approximately $\overline{U_j}/U_\infty = 1$. Increasing $\overline{U_j}$ beyond U_∞ initially causes a small increase in C_D. These results imply that while flow reattachment depends on primarily on meeting a threshold value of C_μ, the blowing ratio could play an important role towards reaching maximum drag reduction.

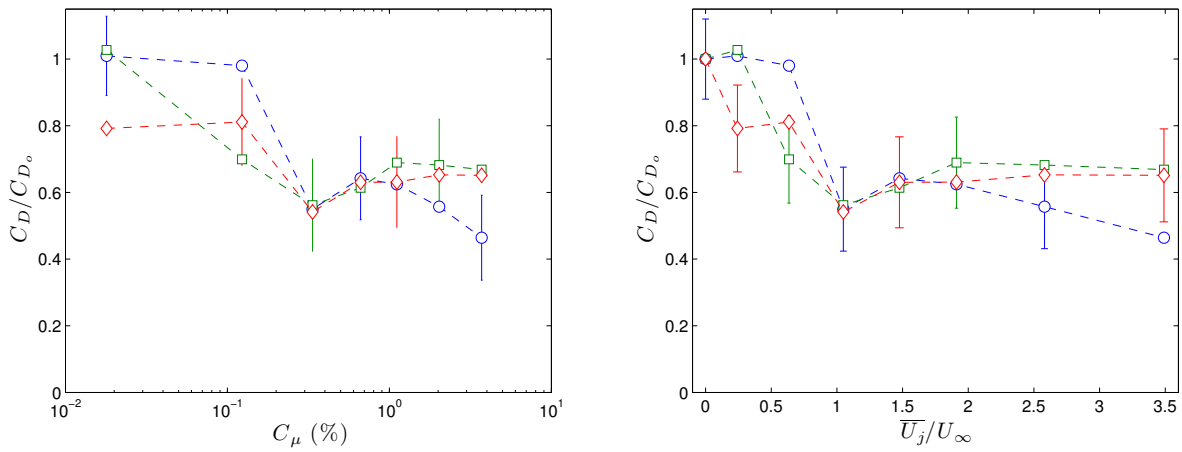

(a) (b)

Figure 14: C_D as a function of (a) C_μ and (b) $\overline{U_j}/U_\infty$ for (○) St_e=58, (□) St_m=0.84 and (◇) St_m=9.9.

4 Conclusions

Synthetic jet actuation was used to mitigate flow separation and improve the aerodynamic performance of a stalled NACA 0025 airfoil. Two actuation strategies were considered: high-frequency and low-frequency excitation. Low-frequency excitation was used to excite the natural instabilities present in the fully separated flow, *viz.* the local shear layer instability (St_{sl}) and global wake instability (St_{ws}).

s High frequency excitation was performed at $St_e = 58$, the lowest resonant frequency of the SJA. As C_μ was increased to 0.34%, a threshold value of C_μ was reached that caused the wake to narrow and shift downwards towards the trailing edge. These changes corresponded to steady reattachment of the boundary layer to the airfoil surface. This reattachment was accompanied by a decrease in C_D of $\sim 45\%$. The peak in power spectra of the cross-stream velocity at $St_{ws} = 0.84$ was suppressed for the reattached flow and at large values of C_μ, a new peak associated with smaller-scale vortex shedding in the wake at $St_{wa} = 4.86$ emerged. Prior to suppression of the large scale shedding in the wake at St_{ws}, a momentary increase in vortex strength occurs that is likely due to a step change in circulation, as found from the wavelet power spectrum of v.

Excitation at the frequency of the wake instability ($St_m = 0.84$) was found to be slightly more effective than high St_e excitation, however the large scale vortex shedding at St_{ws} is no longer suppressed and becomes more organized. At St_m=9.9, the flow was reattached for $C_\mu = 0.018\%$, an order of magnitude less than the threshold C_μ for high frequency excitation. The large-scale vortex shedding in the wake was suppressed for $St_m = 9.9$. For both $St_m = 0.84$ and 9.9, C_D was decreased by $\sim 30\%$ once the threshold C_μ was achieved. Interestingly, both high-frequency and low-frequency excitation caused a local minimum in C_D at $C_\mu = 0.34\%$ where $\overline{U_j}/U_\infty \approx 1$. The duty cycle was fixed at 50% for this work, however the effect of this parameter on flow reattachment is also of interest since the energy required by the SJA scales with DC.

Acknowledgements

The authors gratefully acknowledge support from the Natural Sciences and Engineering Research Council of Canada and the Ontario Graduate Scholarship Program.

References

[1] P. B. S. Lissaman. Low-Reynolds-Number Airfoils. *Annual Review of Fluid Mechanics*, 15:223–239, 1983.

[2] Ari Glezer. Some aspects of aerodynamic flow control using synthetic-jet actuation. *Philosophical Transactions of the Royal Society A: Mathematical, Physical and Engineering Sciences*, 369(1940):1476–1494, 2011.

[3] Barton L. Smith and Ari Glezer. The formation and evolution of synthetic jets. *Physics of Fluids*, 10: 2281, 1998.

[4] David Greenblatt and Israel J. Wygnanski. The control of flow separation by periodic excitation. *Progress in Aerospace Sciences*, 36(7):487–545, 2000.

[5] Jie-Zhi Wu, Xi-Yun Lu, Andrew G Denny, Meng Fan, and Jain-Ming Wu. Post-stall flow control on an airfoil by local unsteady forcing. *Journal of Fluid Mechanics*, 371(1):21–58, 1998.

[6] Ye Tian, Louis Cattafesta, and Rajat Mittal. Adaptive control of separated flow. In *44th AIAA Aerospace Sciences Meeting and Exhibit*, Reno, Nevada, AIAA 2006-1401.

[7] Michael Amitay and Ari Glezer. Role of actuation frequency in controlled flow reattachment over a stalled airfoil. *AIAA Journal*, 40(2):209–216, 2002.

[8] Michael Amitay and Ari Glezer. Controlled transients of flow reattachment over stalled airfoils. *International Journal of Heat and Fluid Flow*, 23(5):690–699, 2002.

[9] Michael Amitay, Douglas R. Smith, Valdis Kibens, David E. Parekh, and Ari Glezer. Aerodynamic Flow Control over an Unconventional Airfoil Using Synthetic Jet Actuators. *AIAA Journal*, 39(3):361–370, 2001.

[10] Ari Glezer, Michael Amitay, and Andrew M Honohan. Aspects of low-and high-frequency actuation for aerodynamic flow control. *AIAA Journal*, 43(7):1501–1511, 2005.

[11] Jeremy T Pinier, Julie M Ausseur, Mark N Glauser, and Hiroshi Higuchi. Proportional closed-loop feedback control of flow separation. *AIAA Journal*, 45(1):181–190, 2007.

[12] Sebastian D. Goodfellow, Serhiy Yarusevych, and Pierre E. Sullivan. Momentum coefficient as a parameter for aerodynamic flow control with synthetic jets. *AIAA Journal*, 51:623–631, 2013.

[13] B Nishri and I Wygnanski. Effects of periodic excitation on turbulent flow separation from a flap. *AIAA journal*, 36(4):547–556, 1998.

[14] Serhiy Yarusevych, Pierre E. Sullivan, and John G. Kawall. Coherent structures in an airfoil boundary layer and wake at low Reynolds numbers. *Physics of Fluids*, 18(4):044101, 2006.

[15] Ye Tian, Qi Song, and Louis Cattafesta. Adaptive feedback control of flow separation. *AIAA paper*, 3016(2006), 2006.

[16] Chungsheng Yao, Fang Jenq Chen, Dan Neuhart, and Jerome Harris. Synthetic jet flow field database for cfd validation. *AIAA paper*, 2218:2004, 2004.

[17] BH Carmichael. *Low Reynolds number airfoil survey.* National Aeronautics and Space Administration, Langley Research Center, 1981.

[18] Savas Yavuzkurt. A guide to uncertainty analysis of hot-wire data. *ASME Transactions Journal of Fluids Engineering*, 106:181–186, 1984.

[19] R. Antonia and S. Rajagopalan. Determination of Drag on a Circular Cylinder. *AIAA Journal*, 28(10): 1833–1834, 1990.

[20] Cornelis P. Van Dam. Recent experience with different methods of drag prediction. *Progress in Aerospace Sciences*, 35(8):751–798, 1999.

[21] Bas W van Oudheusden, Fulvio Scarano, Eric WM Roosenboom, Eric WF Casimiri, and Louis J Souverein. Evaluation of integral forces and pressure fields from planar velocimetry data for incompressible and compressible flows. *Experiments in Fluids*, 43(2-3):153–162, 2007.

[22] James H Mabe, Frederick T Calkins, B Wesley, R Woszidlo, L Taubert, and I Wygnanski. Single dielectric barrier discharge plasma actuators for improved airfoil performance. *Journal of Aircraft*, 46 (3):847–855, 2009.

[23] Martiqua L Post and Thomas C Corke. Separation control on high angle of attack airfoil using plasma actuators. *AIAA Journal*, 42(11):2177–2184, 2004.

[24] David Greenblatt, Keith B Paschal, Yao Chung-Sheng, and Jerome Harris. Experimental investigation of separation control part 2: Zero mass-flux oscillatory blowing. *AIAA Journal*, 44(12):2831–2845, 2006.

[25] Sebastian D. Goodfellow. *Active Flow Control Using Synthetic Jet Actuation*. PhD thesis, University of Toronto, 2010.

[26] LH Benedict and RD Gould. Towards better uncertainty estimates for turbulence statistics. *Experiments in Fluids*, 22(2):129–136, 1996.

[27] BM Jones. *Measurement of Profile Drag by the Pitot-Traverse Method*. ARC R&M 1688, 1936.

[28] Anatol Roshko. On the development of turbulent wakes from vortex streets. *National Advisory Committee for Aeronautics*, 1954.

[29] Wei L. Siauw, Jean-Paul Bonnet, Jean Tensi, Laurent Cordier, Bernd R. Noack, and Louis Cattafesta. Transient dynamics of the flow around a NACA 0015 airfoil using fluidic vortex generators. *International Journal of Heat and Fluid Flow*, 31(3):450–459, 2010.

[30] Serhiy Yarusevych, John G. Kawall, and Pierre E. Sullivan. Separated-Shear-Layer Development on an Airfoil at Low Reynolds Numbers. *AIAA Journal*, 46(12):3060–3069, 2008.